Air–Water CO$_2$ Fluxes in a Highly Heterotrophic Estuary

Susana Flecha · I. Emma Huertas · Gabriel Navarro ·
Edward P. Morris · Javier Ruiz

Abstract Estuaries are hotspots of intense biogeochemical cycling that regulate land–ocean exchanges and support a broad range of ecosystem services. They are a particularly important, still under-resolved, component of the global carbon cycle and often flash points for local socioeconomic conflicts. The mesotidal Guadalquivir estuary is fed by one of the Iberian Peninsula's largest rivers, has a long history of anthropogenic manipulation, and hosts a surrounding population of over 1.7 million people. Monthly sampling of water biogeochemical properties (pigments, nutrients, alkalinity, pH, dissolved oxygen, and organic matter) was carried out in the estuary at 12 stations along its length between November 2007 and August 2009. pCO$_2$ and dissolved inorganic carbon were calculated from total alkalinity and pH, allowing air–water fluxes (FCO$_2$) and land–ocean transport to be estimated. The spatial distribution of oxygen concentration and suspended materials led to divide the system in three zones, the inner estuary (IE), the middle estuary (ME), and the lower estuary (LE), with a minimum oxygen zone and a maximum turbidity zone being found in the IE and ME, respectively. CO$_2$ exchange pattern defined the estuary as a strong source being the IE the major contributor. Thus, estuarine waters were CO$_2$ oversaturated with respect to the atmosphere during most of the study period, with average annual FCO$_2$ values being 66.9 ± 18.6, 29.4 ± 20.3, and 3.4 ± 8.1 mmol C m^{-2} day^{-1} in the IE, ME, and LE, respectively. The average annual CO$_2$ flux to the atmosphere was 36.4 ± 11.7 mol C m^{-2} year^{-1}. The present study reinforces the heterotrophic status of the estuary in relation to the carbon system variable description.

S. Flecha (✉) · I. E. Huertas · G. Navarro · E. P. Morris · J. Ruiz
Instituto de Ciencias Marinas de Andalucía, Consejo Superior de
Investigaciones Científicas (ICMAN-CSIC), Polígono Río San
Pedro, Puerto Real 11510, Cádiz, Spain
e-mail: susana.flecha@icman.csic.es

Introduction

Estuaries, due to their transition location, are affected by both marine processes, such as tides, waves, and intrusion of saline water, and riverine processes like flows of freshwater and sediments. They also represent an important source of nutrients to the coastal area, as estuarine systems are considered regions of a high productivity worldwide (Mann 1982). Nutrient inputs in estuaries (particularly nitrate) are affected by water discharge, entries from both natural (groundwater transport, riverine inflow, and atmospheric deposition) and anthropogenic sources (sewage treatment plants, agricultural and lawn fertilizers, etc.), and resident estuarine processes, such as denitrification and nitrification (Soetaert et al. 2006).

Elevated nutrient concentrations spur rapid phytoplankton growth and the occurrence of periodic microalgal blooms that eventually lead to the generation of considerable organic loads. Subsequent bacterial decomposition of this organic matter promotes oxygen depletion, and thus hypoxic or anoxic zones may commonly appear in estuaries (Conley et al., 2009). The genesis of hypoxia can be traced by specific nitrogen compounds, as nitrification processes decrease oxygen concentration, and denitrification principally proceeds in suboxic conditions. Hypoxia in estuaries represents a common disturbance (Cox et al., 2009; Sharp, 2010) causing death of biota and catastrophic changes at the entire ecosystem level (Vaquer-Sunyer and Duarte, 2008). Not only organisms and their habitat are affected by hypoxia but also the biogeochemical processes that control nutrient concentrations in the water column (Conley et al., 2009). Moreover, turbulence induced by the meeting of the downstream freshwater flow and the upstream tidal flow and flocculation of material induced by

the mixing of fresh and salt water increase residence times of suspended particulate matter (SPM), forming maximum turbidity zones (MTZ), which are generally considered the most important regions in a tidally influenced estuary, where photosynthesis becomes strongly limited by light availability (Abril et al., 1999; Amann et al., 2012; Etcheber et al., 2007; Garnier et al., 2010; Herman and Heip, 1999). Heterotrophic activity is in turn enhanced ought to the high turbidity, resulting in a net mineralization of a major part of the particulate organic carbon (POC) (Gattuso et al., 1998). As a final consequence, high levels of CO_2 generated by degradation of dissolved and/or particulate organic carbon and by other anaerobic processes in addition to denitrification, such as sulfate reduction and in some anaerobic environments methanogenesis (Richey et al., 1988), are released to the atmosphere. These kinds of estuaries act then as significant sources of CO_2 to the atmosphere due to their net heterotrophic metabolic status (Frankignoulle et al., 1998; Chen and Borges, 2009; Laruelle et al., 2010; Borges and G. Abril 2011; Chen et al., 2012; Chen et al., 2013; Testa et al., 2013).

Given the complexity of the biogeochemical processes involved in the heterotrophy of estuaries, integrated studies performed at a high spatiotemporal scale are needed to properly characterize the dynamics of these systems. Furthermore, in order to determine the contribution of estuaries to the CO_2 emissions and the horizontal fluxes of carbon, high-resolution data with a proper degree of accuracy are required to obtain and provide precise estimates of the air–water CO_2 exchange in these environments.

Within this context, this work was aimed at examining the temporal and spatial variability of the carbon system parameters in the tidally dominated Guadalquivir estuary (SW Spain, Fig. 1) in relation to the metabolic status of the system. Despite its socioeconomic and environmental significance (Ruiz et al., 2009), until very, recently only one study addressing the characterization of the inorganic carbon system inside the estuary had been published (de la Paz et al., 2007). On other hand, several works have been carried out in the adjacent coastal fringe of the Gulf of Cádiz, where the Guadalquivir River discharges (Huertas et al., 2006; Ribas-Ribas et al., 2013), or in the wetlands of Doñana National Park, located in the northern rim of the lower estuary (Morris et al., 2013). The Guadalquivir estuary is characterized by a strong turbidity (Navarro et al., 2011; Caballero et al., 2013), which markedly restricts light availability for phytoplankton growth (Navarro et al., 2012). Light limitation seems to be a constant feature within the estuary, thereby constraining primary productivity even though high nutrient loads are present in the water column (Navarro et al., 2012; Ruiz et al., 2014). The seasonal shift in hydrology from winter river-dominated (rainfall season) to tidally dominated flow is the main factor controlling the patterns of nutrients and suspended matter in the estuary (Díez-Minguito et al. 2012), as during the river-dominated

period considerable freshwater inputs from an upstream reservoir (the Alcala del Rio dam) are introduced in the system. Due to the relevance of the estuary on its adjacent areas, we assessed the spatiotemporal distribution of carbon system parameters in the system during nearly 2 years of sampling in relation to biogeochemical variables indicative of heterotrophy. The analysis was ultimately aimed at determining the air–water CO_2 exchange in the estuary and the processes governing gas transference.

Material and Methods

Study Area

The Guadalquivir River, located in Southern Spain (Fig. 1), is one of the longest rivers in the Iberian Peninsula, with a total length of 560 km and a drainage area of 57,527 km^2. The estuarine region hosts 1.7 million inhabitants, which are distributed on 90 population settlements (Navarro et al., 2012). Due to the socioeconomic importance of the estuary (agriculture, fisheries, tourism, etc.), it is affected by an intense anthropogenic pressure. Guadalquivir is the only large navigable river in Spain, reaching to the port of Sevilla. Therefore, maintenance activities of the navigation channel take part regularly in the estuary, including lock building and dredging works to deepen the main channel, in order to allow big ships the access into Seville's port (Ruiz et al., 2014).

The estuary extends to the Alcala del Rio dam, which is situated 110 km upstream from the river mouth, being characterized by a main channel surrounded by tidal creeks with a few significant little intertidal zones. As a mesotidal system, the tidal influence is noticeable up to the dam, and the maximum tidal range at river mouth is 3.5 m during spring tides (Díez-Minguito et al., 2012).

The basic climate in the region is Mediterranean, defined by warm temperatures (16.8 °C annual average) and with relatively short periods of heavy rainfall occurring during winter (annual average of 550 l m^{-2}). The Atlantic Ocean orientation allows storms entering from West, driving the distribution of rainfall SW–NE. The rainfall often adopts torrential character acting on a system recurrently affected by long dry periods, high temperatures, and consequently with a marked erosion susceptibility (Memoria de la Confederación Hidrográfica del Guadalquivir 2009/2011, Ministerio de Agricultura, Alimentacion y Medioambiente, Gobierno de España).

Sampling Strategy

Monthly samplings were carried out at 12 stations between November 2007 and August 2009 (Fig. 1). From station 1 positioned at the river mouth, stations 2 to 12 were located at

Fig. 1 Location of the study area, sampling sites, and meteorological stations. Position of the Alcala del Río dam is also shown
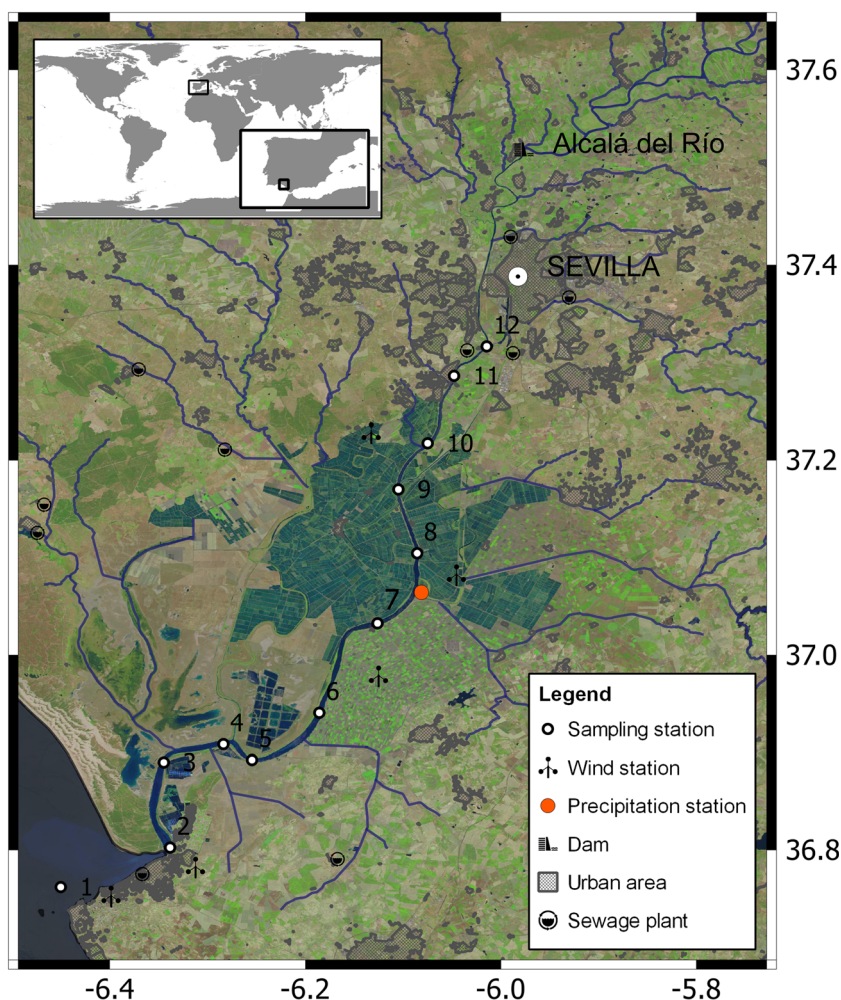
6, 16, 22, 25, 34, 46, 55, 63, 71, 78, and 82 km upstream, respectively. At each station, conductivity, temperature, and depth (CTD), salinity, and turbidity profiles were obtained with a Sea-Bird SBE 19 plus equipped with a Turbidimeter Cyclops-7 sensor (Turner Designs), which was followed by collection of water samples at 1-m depth with a Van Dorn bottle sampler for the determination of the following biogeochemical variables: total alkalinity (A_T), pH, dissolved oxygen (DO), SPM, chlorophyll (Chl$a$), inorganic nutrients (NH_4^+, NO_2^-, NO_3^-, PO_4^{-3}, and Si), dissolved organic carbon (DOC), and total dissolved nitrogen (TDN).

Measurement Protocols

Water samples for A_T determination were collected in 500-ml borosilicate bottles and poisoned with 100 μl of $HgCl_2$-saturated aqueous solution until analysis in the laboratory according to the DOE handbook protocols (Dickson and C. Goyet 1994). A_T was measured by potentiometric titration with a Metrohm 794 Titroprocessor using the method described by Mintrop et al. (1999). The precision and accuracy of A_T

determinations were between ±5.3 and 2.1 μmol kg^{-1}, respectively, as determined from daily measurements of two batches (#94 and #97, $n=44$) of certified reference material (CRM, supplied by Prof. Andrew Dickson, Scripps Institution of Oceanography, La Jolla, CA, USA). Constants used for A_T calculations as for boric acid and $KHSO_4$ were those from Cai and Wang (1998), Lee et al. (2010), and Dickson (1990b), respectively. Water pH measurements in the National Bureau of Standards (NBS) scale (pH$_{NBS}$) were carried out from the A_T samples using a Metrohm 780 pH meter equipped with a combined glass electrode. Calibrations were conducted daily using NBS buffers at three different pH values, 4, 7, and 9. Precision and accuracy of the pH measurements were 0.001 and ±0.003 pH units, respectively.

Dissolved oxygen was measured using an automated potentiometric modification of the original Winkler method following WOCE standards (WOCE 1994). Flasks containing the water samples were sealed, stored in darkness, and measured within 24 h. Dissolved oxygen concentrations were derived using the Metrohm 794 Titroprocessor, with an estimated error of ±2 μmol l^{-1} ($n=115$).

SPM as well as particulate organic matter (POM) and particulate inorganic matter (PIM) were determined by using the loss on ignition (LOI) method. A known volume of water was filtered through pre-combusted 450 °C Whatman GF/F glass fiber (0.7 mm pore size). Filters were dried at 60 °C for 48 h and weighed to derive SPM (g l^{-1}), further combusted at 450 °C for 5 h, and weighed to derive PIM and POM by difference.

Chlorophyll analysis was conducted by filtering known volumes of water through Whatman GF/F glass fiber filters, extracting in 90 % acetone overnight in the dark, and measuring chlorophyll a concentrations (Chl$a$) by fluorometry with a Turner Designs 10-AU Model fluorometer according to the Joint Global Ocean Flux Study (JGOFS) protocol (Knap et al., 1996b). The fluorometer was calibrated using a pure Chl$a$ standard from the cyanobacterium *Anacystis nidulans* (Sigma Chemical Company).

Inorganic nutrient sampling was performed following the methodology described by Knap et al. (1996a). Two 5-ml samples of filtered water (Whatman GF/F glass fiber) were obtained and stored at −20 °C until analysis. Concentrations of NH_4^+, NO_2^-, NO_3^-, PO_4^{-3}, and Si were derived following the techniques described by Grasshoff et al. (1983) using a Skalar San++ 215 Continuous Flow Analyzer. For the analysis of DOC and TDN, water samples were collected in borosilicate vials (pre-acid-washed and combusted, 450 °C). Water was filtered with pre-combusted 450 °C Whatman GF/F glass fiber, 47-mm filters and 24-ml subsamples were acidified with 50 µl of 25 % H_3PO_4, sealed, and conserved at 4 °C in darkness until analysis. Samples for DOC and TDN were obtained according a modification of the JGOFS protocol (Knap et al., 1996a). Concentrations of DOC and TDN were derived by catalytic oxidation at high temperature (720 °C) and chemiluminescence, respectively, by using a Shimadzu TOC-VCPH analyzer. TDN was subsequently used to obtain dissolved organic nitrogen (DON) concentrations by subtracting inorganic nitrogen (Álvarez-Salgado and Miller, 1998).

The diffuse attenuation coefficient for photosynthetically active radiation (PAR) was calculated by the following expression obtained from Gallegos (2001):

$$K_d = K_w + K_c[Chla] + K_s[SPM] \tag{1}$$

where K_w (0.26 m^{-1}) is the attenuation due to water alone, and K_C (0.017, (m^2 (mg Chl)$^{-1}$) and K_S (0.074 m^2 g^{-1}) stand for the specific attenuation coefficient of chlorophyll and SPM, respectively. The diffuse attenuation coefficient (K_d) was used to estimate the lower limit of the euphotic zone ($Z_{1\%}$) defined as the depth where the PAR represents 1 % of the surface radiation, following the Lambert-Beer law (Kirk, 1994):

$$Z_{1\%} = Ln(0.01)/K_d \tag{2}$$

Calculations of Air–Water CO_2 fluxes

For flux calculations, $[pCO_2]_{water}$ and dissolved inorganic carbon (DIC) were obtained from A_T and pH_{NBS} pairs by using the CO2SYS software (Lewis et al., 1998) with the thermodynamic equations and constants for carbon and sulfate of Cai and Wang (1998) and Dickson (1990a), respectively.

Air–water CO_2 fluxes (FCO$_2$ in mmol CO_2 m^{-2} day^{-1}) were calculated according to Wanninkhof et al. (2009):

$$FCO_2 = k_w k_0 \left([pCO_2]_{water} - [pCO_2]_{air} \right) \tag{3}$$

where k_w (m s^{-1}) is the water side gas transfer velocity, k_0 (mol m^{-3} atm^{-1}) is the aqueous phase solubility of CO_2 at the in situ temperature (°C) and salinity (Weiss 1974; Wanninkhof 1992), and $[pCO_2]_{air}$ in µatm is the atmospheric pCO_2 values obtained from the NOAA Lampedusa (Italy) monitoring station (http://www.esrl.noaa.gov/gmd/dv/site/) and then converted from pCO_2 dry to wet (Weiss and Price, 1980). k_w was calculated using:

$$k_w = k_{600}(S_{cw}/600)^{-0.5} \tag{4}$$

where S_{cw} is the Schmidt number interpolated at the in situ salinity from the freshwater and seawater equations (see Wanninkhof 1992). k_{600} is the gas transfer velocity at a Schmidt number of 600 (often quoted as typical of freshwater at 20 °C). k_{600} was predicted from time ensemble-averaged (1 day) horizontal wind velocity at 10 m above the surface (U_{10} m s^{-1}) using the empirical relationships of Raymond and Cole (2001),

$$k_{600} = 1.58\, e^{0.3}\, U_{10} \tag{5}$$

where k_{600} is in centimeter per hour. U_{10} was calculated from U_z measured at nearby meteorological stations (Estaciones Agroclimaticas, Junta de Andalucia, Spain; Fig. 1) according to Smith (1988). For comparison, k_{600} proposed by Clark et al. (1995) and the recently revised by Jiang et al. (2008) were also used.

Daily discharge data from the Alcala del Rio dam and precipitation from the Lebrija Brazo del Este Station (precipitation station in Fig. 1) were obtained from the Sistema Automático de Información Hidrológica of the Guadalquivir basin (http://www.chguadalquivir.es/saih/Inicio.aspx).

Statistics

Statistics were performed with the statistical program language R 3.02 (R Development Core Team, 2013).

Probability distributions of variables were examined visually and in most cases were log-normal and highly skewed. Nonparametrical Kruskal-Wallis rank sum tests (KWRS, R function; kruskal.test) and nonparametrical multiple test procedures Kruskal-Wallis multiple comparison test (KWMC, Package; pgirmess, function; kruskalmc) were used to examine differences between zones (Giradoux, 2012). Significance levels were set at $p < 0.05$. Principle component analysis (R package; FactoMineR, function; PCA, Husson et al., 2012) of transformed, $\log(x+1)$, variables, with monthly mean wind speed, monthly river discharge, and surface temperature as a supplementary quantitative variables, was used to explore correlations. Linear regressions between variables were also used to establish linear relationships.

Results and Discussion

### Estuary Partitioning: Spatiotemporal Distribution of Thermohaline Properties

PCA revealed that data could be summarized into five components that accounted for a cumulative percentage variance of 77 % (Fig. 2), with values from PC1 to PC5 of 30.73, 19, 11.54, 8.75, and 6.63 %, respectively. In terms of briefly characterizing, only principle components 1 (PC1, Dim 1) and 2 (PC2, Dim 2) are discussed here. PC1 appears to represent spatial distribution and thus led us to divide the estuary in three regions. Positive PC1 values (Fig. 2a) mainly represented higher values of dissolved material (A_T, DOC, and DON) corresponding to stations 9 to 12 (Fig. 1; Table 1), which then defined the inner

estuary (IE). Negative PC1 (Fig. 2a) appears to represent elevated values of salinity, DO, and pH corresponding to stations 1 and 2 (Fig. 1; Table 1), characterizing hence the lower estuary (LE). The transitional zone between the inner and lower estuary, comprising stations 3 to 8 (Fig. 1), was then designed as the middle estuary (ME). IE was characterized by the presence of the lowest dissolved oxygen concentrations (Fig. 3) representing thus the oxygen minimum zone (OMZ). During our study, oxygen levels were as low as 1.1 mg l^{-1}, suggesting that OMZ can, at times, be classified as severely hypoxic. As defined by the Environmental Protection Agency (EPA, 2000), hypoxia in aquatic ecosystems occurs at oxygen levels below 2.9 mg l^{-1}, with severe hypoxia being marked by concentrations <2.3 mg l^{-1}. In contrast, oxygen levels in the ME and LE were ~6 mg l^{-1} in both zones.

Salinity range in the IE was mesohaline, with salinity values <5 (Fig. 3 and Table 1), which progressively increased throughout the estuary to finally reach 36 in the river mouth (LE, Fig. 3). The spatial distribution of salinity within the entire estuary may be attributed to the combination between the tidal flooding and variability in river discharge from the dam (Navarro et al., 2012; Díez-Minguito et al. 2013).

In addition to salinity linked to PC1 (Fig. 2b), turbidity was also selected as a variable defining spatial variability, due to its relevance on the ecosystem dynamics (Navarro et al., 2012; Ruiz et al., 2014). Turbidity maximum was located within the ME, defining the MTZ (Fig. 3 and Table 1).

On the other hand, PC2 seems to describe seasonal variations during the study period, as negative values represent high temperature and Chl$a$, both mostly appearing during spring–summer (Fig. 2b). Conversely, positive values define autumn–winter conditions with increased precipitations and particulate matter (PM) contents. The highest spatial
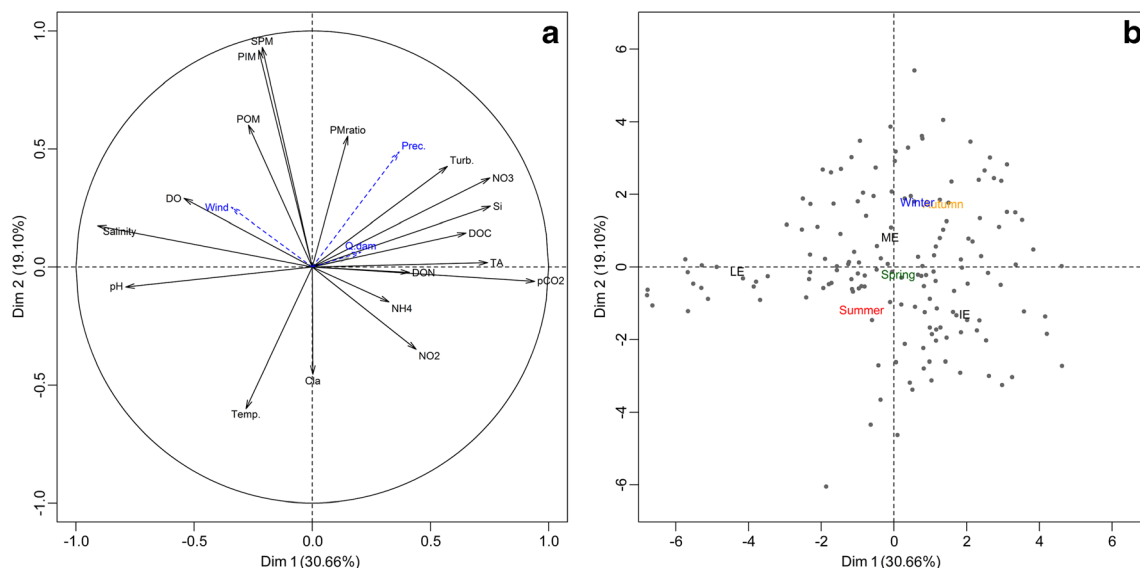
Fig. 2 Biplots of water physical and chemical characteristics with scaling highlighting variable correlations (**a**) and mapping of individual samples (**b**). Rainfall, wind velocity, and Alcala del Rio dam discharge are plotted as supplementary variables (*blue arrows and text*) on **a**. Text representing the centroids for lower estuary (*LE*), middle estuary (*ME*), and inner estuary (*IE*) and seasons are shown on **b**

Fig. 3 Average values of salinity, dissolved oxygen (mg l⁻¹), and turbidity in Formazin Nephelometric Units (*FNU*) along the estuary, defining the three areas in which the estuary has been divided: LE, ME, and IE
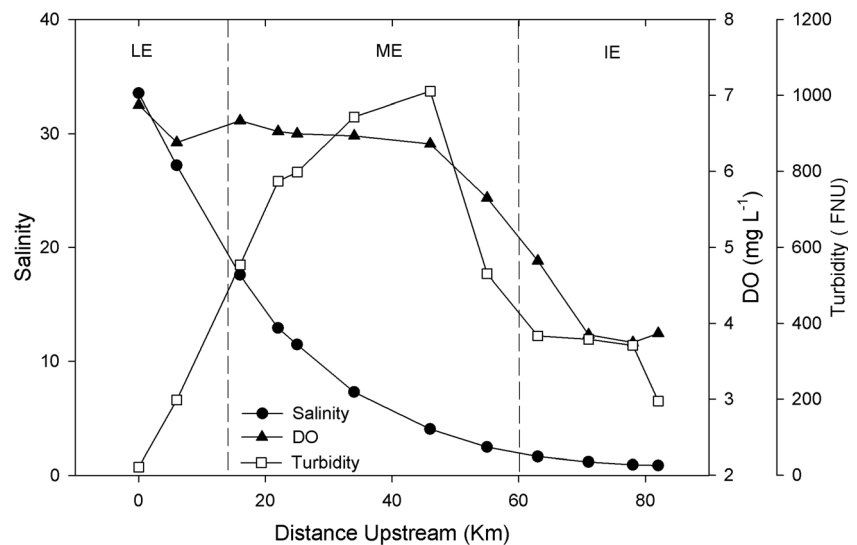
variability was found invariably in the ME, whereas at a temporal scale, spring season seemed to be the most fluctuating period for the whole estuary (Fig. 2b).

Surface water temperature pattern was typical of the Mediterranean climate area, with hot summers and moderate cold winters. During the study period, water temperature values ranged from 4.6 to 27.7 °C (Table 1), with no statistical differences between zones (KWRS $\chi^2=2.2$, degrees of freedom (df)=2, p value>0.05). In contrast, neither salinity nor dissolved oxygen values presented any seasonal variation (KWRS p value>0.05).

Chlorophyll, Turbidity, Water Discharge, and Light Penetration

Guadalquivir estuary can be categorized as one of the most turbid rivers in the world, with average SPM values of 650.5 mg l⁻¹ (Table 1). For instance, rivers such as Huanghe (China), Mackenzie River (Canada), Amazon (Brazil), and the Scheldt estuary (Belgium) have mean SPM concentrations of 23, 830, 320, 97, and 100 mg l⁻¹ (Gaillardet et al., 1999; Kim et al., 2010; Chen et al., 2005), respectively. This is also shown by the turbidity values provided by the CTD sensor (Table 1), which markedly varied along the different zones of the estuary (KWRS $\chi^2=63.1$, $df=2$, p value<0.001). The high turbidity in the Guadalquivir estuary can be related to the generally long residence time and with the occurrence of high mesotidal currents (Díez-Minguito et al., 2012; 2013).

As illustrated in Fig. 4b, K_d values manifestly changed throughout the year (KWRS $\chi^2=39.1$, $df=3$, p value <0.001), with a maximum of 400 m⁻¹ reached in spring 2009 and a minimum of 1.5 m⁻¹ in autumn 2008, resulting in changes in the euphotic depth from −0.01 to −3.1 m⁻¹ (Fig. 4c). Maximum K_d values were generally observed during periods of high precipitation or high discharges from the Alcala del Rio dam (Fig. 4a, b). When high loadings occurred, light penetration was more limited, and hence the lower limit of the euphotic zone shallowed (Fig. 4b). As a result, primary production was expected to be highly restricted due to reduced

Table 1 Average values, standard deviation, and number of observations in brackets (*n*) of the variables presented in this study for the three areas defined in the Guadalquivir estuary

	Lower estuary (*n*=38)	Middle estuary (*n*=134)	Inner estuary (*n*=75)
Area (km²)	40.1	23.8	7.2
Temperature (°C)	18.5±4.6	18.2±5.3	19.3±5.8
Salinity	30.0±6.4	9.2±6.8	1.1±0.6
Turbidity (FNU)	111±376	769±1,116	310±271
DO (mg l⁻¹)	6.6±1.0	6.4±1.3	4.0±1.6
pH_{NBS}	8.2±0.1	8.0±0.2	7.8±0.2
A_T (µmol kg⁻¹)	2,633±273	3,468±403	3,505±328
DIC (µmol kg⁻¹)	2,613±285	3,442±389	3,523±300
pCO_2 (ppm)	477±319	1,440±807	3,009±958
PO_4^{3-} (µM)	1.5±1.1	2.7±1.0	2.2±1.4
Si (µM)	42.5±38.0	112.5±30.3	122.7±36.3
NO_3^- (µM)	99.0±103.3	302.8±154.9	390.3±162.4
NO_2^- (µM)	0.9±1.5	1.1±2.6	5.9±5.4
NH_4^+ (µM)	5.3±3.6	5.2±8.3	19.1±49.4
DOC (mg l⁻¹)	3.8±1.7	6.0±1.6	6.9±2.8
DON (mg l⁻¹)	15.1±21.7	61.8±56.8	92.6±90.6
Chl*a* (µg l⁻¹)	2.9±3.2	1.8±1.4	3.3±3.5
SPM (mg l⁻¹)	771±504	779±790	360±372
PIM (mg l⁻¹)	667±473	679±708	310±355
POM (mg l⁻¹)	104±44	100±199	50±43
K_d (m⁻¹)	55.9±38.0	57.9±57.5	26.6±27.5

Fig. 4 Time distribution in the Guadalquivir estuary of **a** daily averaged discharge (m³ s⁻¹) in *gray* and precipitation (l m⁻²) in *dotted red*, **b** light extinction coefficient, K_d (m⁻¹), **c** euphotic zone, $Z_{1\%}$ (m⁻¹), and **d** chlorophyll *a*, Chl*a* (µg l⁻¹). *Gray* background bands highlight the periods with higher discharges in the estuary during the time of the study. The *tops* and *bottoms* of each "box" are the 25th and 75th percentiles of the samples, respectively. The distances between the tops and bottoms are the interquartile ranges. The *line in the middle of each box* is the sample median. Observations beyond the whisker length are marked as outliers displayed with a *black dot*
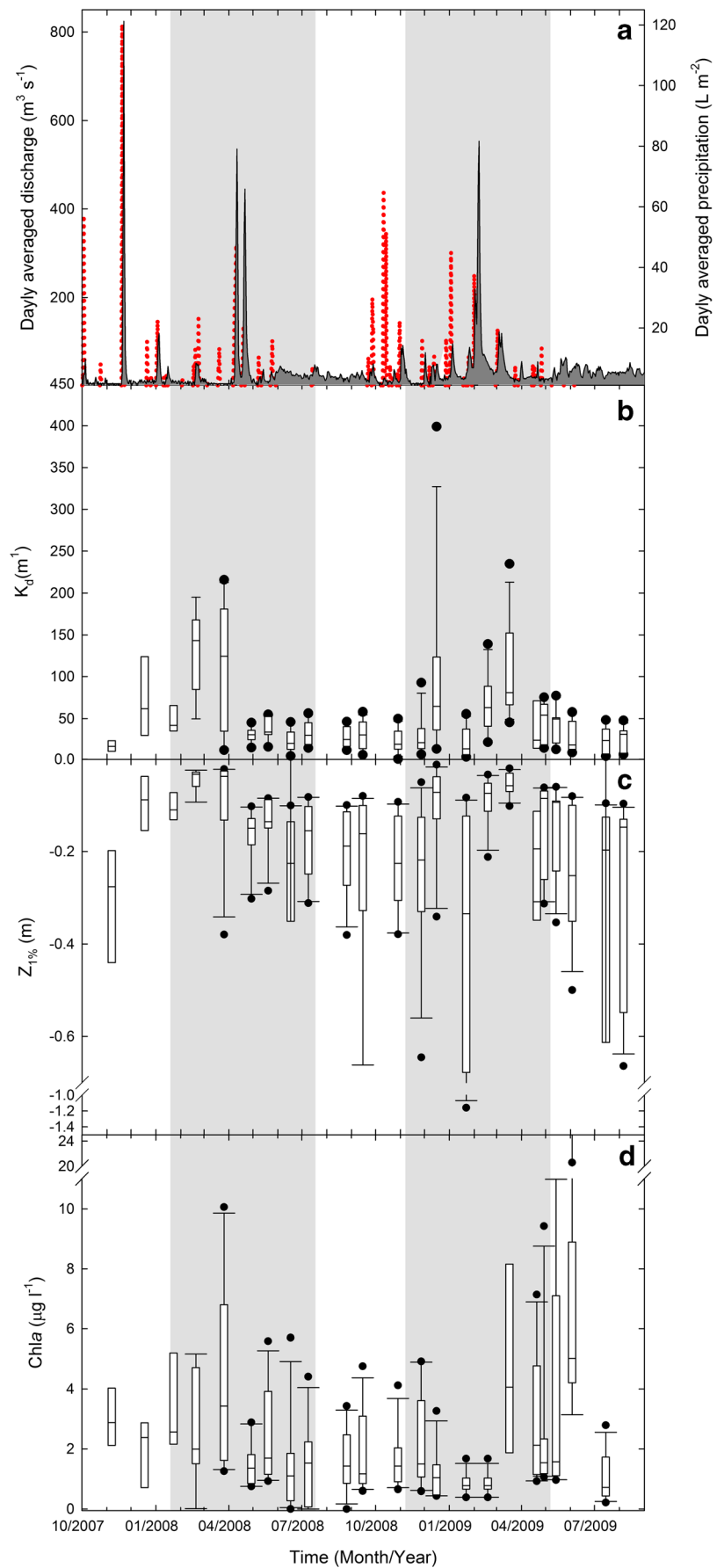
light availability, and as seen also in Taglialatela et al. (2012), zooplankton dominant species decreased to extremely low values during these events.

Chl$a$ appeared to exhibit a seasonal trend (Fig. 4d), with spring blooms in 2008 and 2009 with maxima of 10 µg l^{-1} and the lowest concentrations around 0.1 µg l^{-1} during autumn and winter coinciding with increased precipitations and discharges. Nevertheless, Chl$a$ concentrations were lower than the expected phytoplankton biomass that could be supported by the nutrient levels present in the estuary (Ruiz et al., 2014), feature that can be attributed to light limitation, as shown by the K_d and $Z_{1\%}$ values, which indicate that light penetrated on average only 5 % into the water column.

Carbon System Parameters

Total alkalinity, plotted in Fig. 5a, was characterized by a marked spatial variability (KWRS χ^2=83.5, df=2, p value< 0.001), with the highest values measured being associated with the transition between IE and ME (KWMC p<0.05). Minimum A_T concentrations were found in the LE, as the proximity to the coastal area allows the inflow of seawater characterized by a lower A_T. In fact, in this part of the estuary, the mean alkalinity during the whole study period was 2,632.52±272.82 µmol kg^{-1} (Table 1), similar to that measured in the continental shelf of the Gulf of Cádiz and equivalent to 2,402.5±8 and 2,360±2 (Ait-Ameur and Goyet, 2006; Flecha et al., 2012). In contrast, waters with higher alkalinity were found upstream, with average values of 3,468.18±403.15 and 3,505.33±327.98 µmol kg^{-1} in the ME and IE, respectively. As reported previously by de la Paz et al. (2007), this alkalinity pattern can be partially related to the carbonate materials presented in the drainage basin of the upper part of the estuary (Pérez-Hidalgo and Trinidad, 2004) and the mixing between fresh and marine waters. A_T values did not present any seasonal variation during the study period (Table 1).

The distribution of pH$_{NBS}$ values also exhibited a strong spatial (KWRS χ^2=95, df=2, p value<0.001) and temporal variability (KWRS χ^2=48.6, df=2, p value<0.001). No statistical differences were observed (KWMC p<0.05) between spring and autumn, whereas significant differences were found among the rest of seasons, with winter being the period in which lower pH$_{NBS}$ values were measured (Table 2). The spatial variability of pH$_{NBS}$ in the IE (Table 1 and Fig. 5b) can be associated to the freshwater discharges from the dam. Conversely, higher pH$_{NBS}$ values found in the LE may reflect the entry of saltier and oxygenated waters as well the influence of the DIC fluxes from the river. In opposition, pCO$_2$ exhibited a gradual increasing gradient upstream (Fig. 5c), as seen

in other estuaries (Chen et al., 2012) and already reported in this system (de la Paz et al., 2007). Extremely high pCO$_2$ concentrations (between 4,000 and 5,000 µatm) were detected in the IE, where pCO$_2$ levels always exceeded 1,000 µatm during the whole study period (Fig. 5c). In the LE, average values also coincide with those measured in previous studies in the area (de la Paz et al., 2007; Ribas-Ribas et al., 2011), presenting during certain short periods, pCO$_2$ values below the atmospheric concentration (Table 1). Nevertheless, our data show that the Guadalquivir estuary, in average, was constantly characterized by pCO$_2$ values higher than the atmospheric concentration (Table 1 and Table 2). These CO$_2$ concentrations are higher in relation to those observed in the past, which fell within a range from 518 to 3,606 µatm from low to high salinity (de la Paz et al., 2007).

Taking salinity as a good indicator for mixing of dissolved compounds subject exclusively to physical processes, a linear relationship between DIC and salinity can be obtained, which allows to estimate the concentration of inorganic carbon in freshwater. Our calculations (DIC=3.68−0.034 S, R^2=0.64, n=248) yield then a value of carbon in freshwater corresponding to 3.68 mmol kg^{-1}, and considering a historic average discharge of 160 m^3 s^{-1} (Ruiz, 2010), the transport of inorganic carbon by advective processes from the Guadalquivir estuary to the continental shelf of the Gulf of Cádiz resulted in 50×10^6 mol C day^{-1}, indicating that the system has the potential to channelize an advective export of approximately 219,000 t of C per year.

Air–Water CO$_2$ Exchange

Fluxes of CO$_2$ between the atmosphere and the water column (FCO$_2$) throughout the Guadalquivir estuary were calculated using three gas transfer velocities (k_{600}) for comparison. No large differences were detected between the outputs obtained with the parameterizations of Clark et al. (1995) and Raymond and Cole (2001), as k_{600} ranged from 2.54 to 7.26 and from 2.13 to 6.69 cm h^{-1}, respectively. In contrast, when the Jiang et al. (2008) parameterization was used, an increase in k_{600} was observed for the whole wind range (from 3.89 to 8.98 cm h^{-1}), as this formulation magnifies the coefficient values for wind speeds below 5 m s^{-1}. Taking into account this caveat and in order to compare with historic data, only fluxes calculated according to Raymond and Cole (2001) were subsequently considered in our study (Fig. 6).

The temporal distribution of FCO$_2$ indicated that estuarine waters were oversaturated with respect to the atmosphere during most of the study period (Fig. 6), with average annual FCO$_2$ values decreasing from 66.9±18.6 to 29.4±20.3 and to 3.4±8.1 mmol C m^{-2} day^{-1} in the IE, ME, and LE,

Fig. 5 a Total alkalinity (μmol kg^{-1}), **b** pH (NBS scale), and **c** pCO$_2$ values (μatm) from the river mouth to 80 km upstream. The *tops* and *bottoms* of each "box" are the 25th and 75th percentiles of the samples, respectively. The distances between the tops and bottoms are the interquartile ranges. The *line in the middle of each box* is the sample median. Observations beyond the whisker length are marked as outliers displayed with a *black dot*
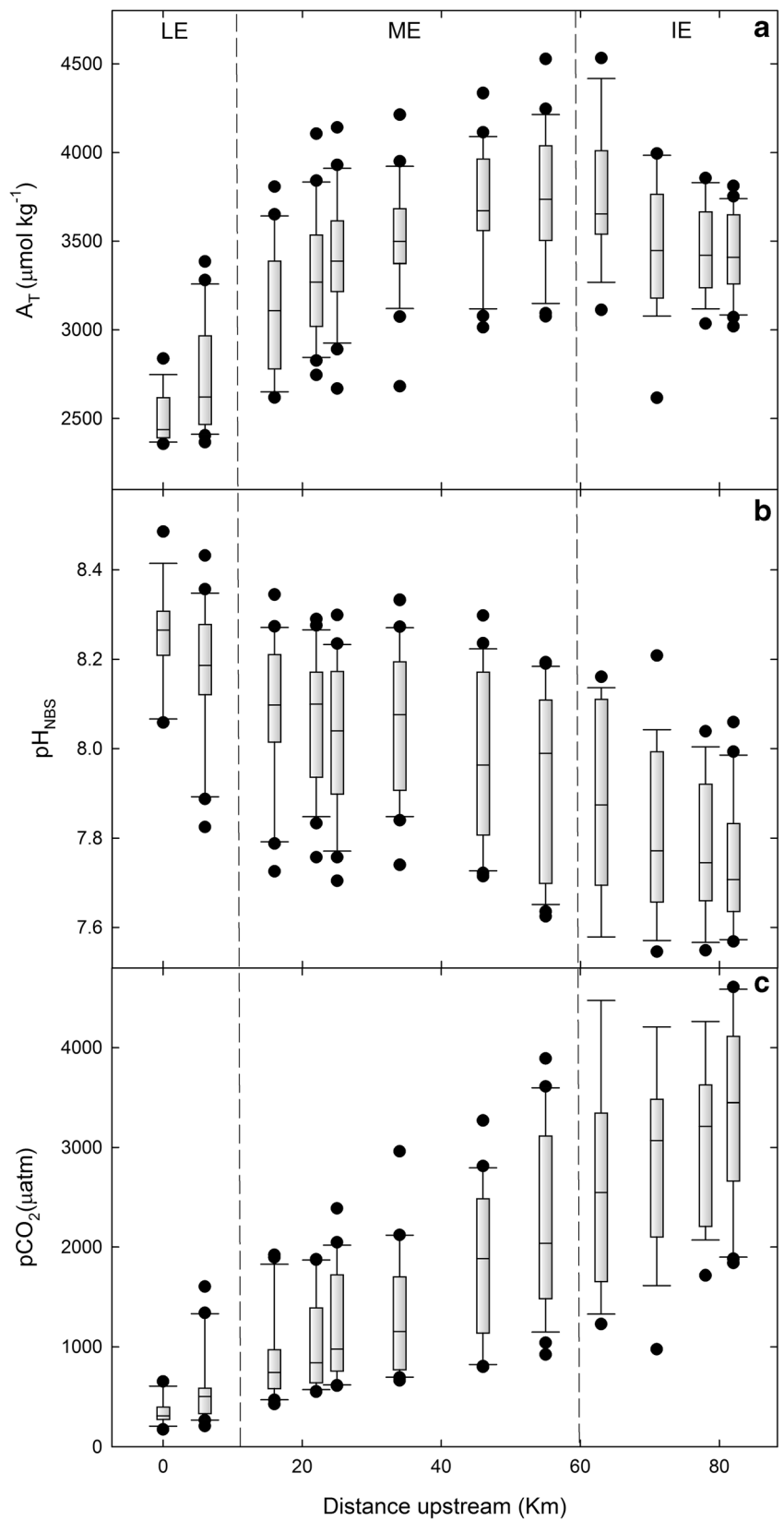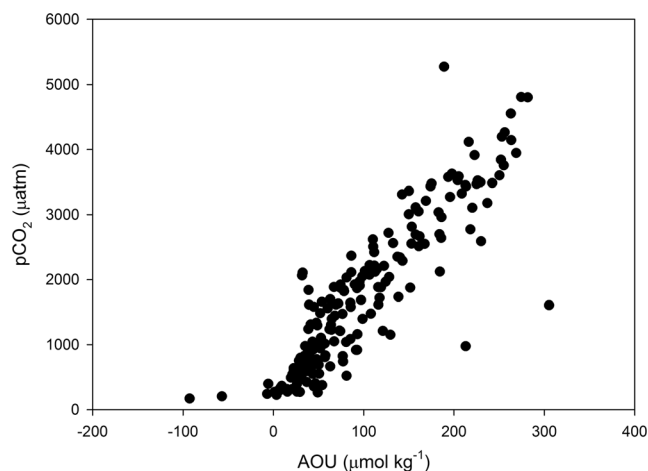
Fig. 6 Spatiotemporal distribution of air–water CO_2 fluxes (FCO_2, mmol m^{-2} day^{-1}) in the Guadalquivir estuary during the study period for the **a** IE, **b**, ME, and **c** LE. Negative FCO_2 values indicate that the area acts as a sink and positives as a source. The *tops* and *bottoms* of each "box" are the 25th and 75th percentiles of the samples, respectively. The distances between the *tops* and *bottoms* are the interquartile ranges. The *line in the middle of each box* is the sample median
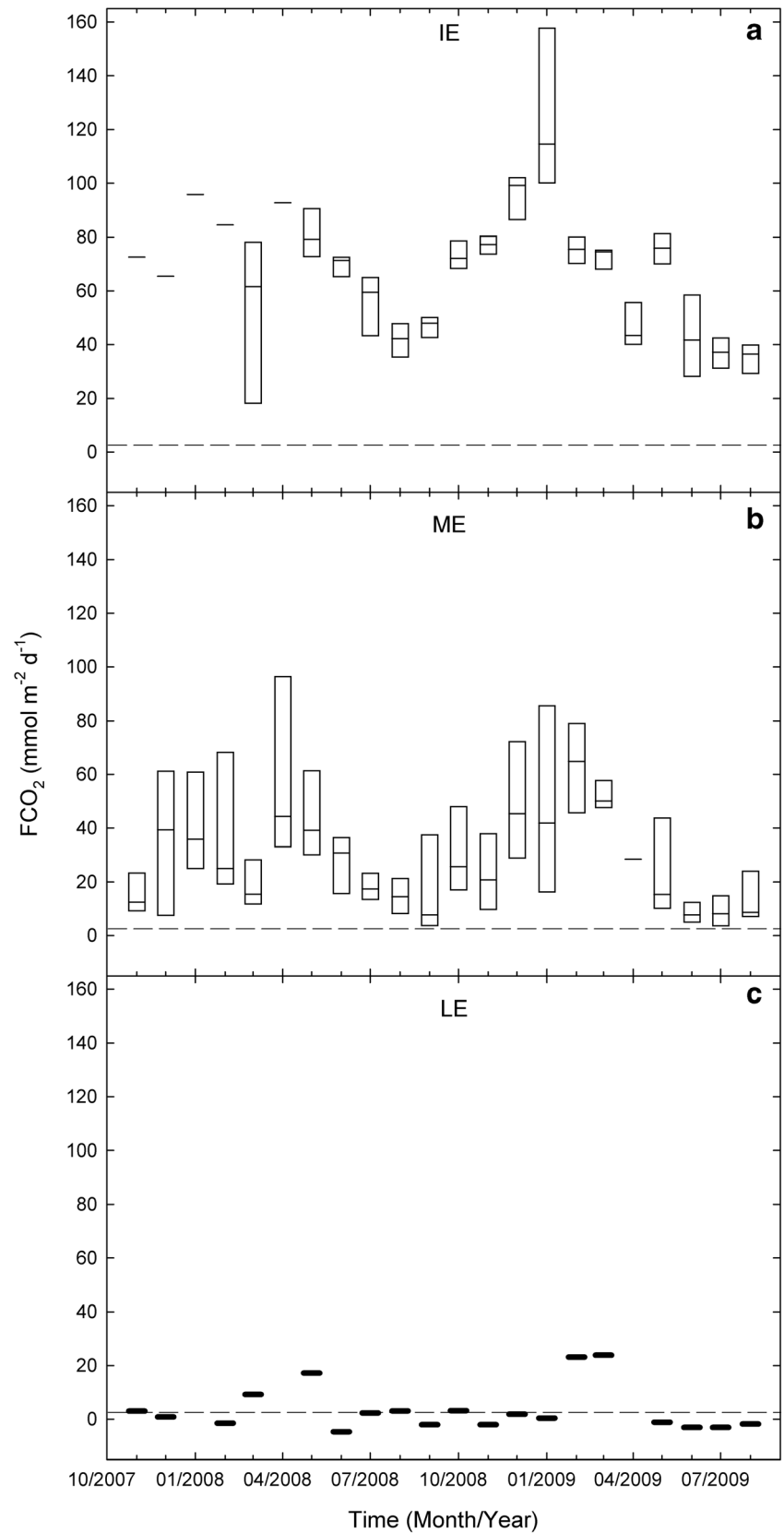
Table 2 Average values, standard deviation, and number of observations in brackets (n) of pH_{NBS} A_T (µmol kg^{-1}), DIC (µmol kg^{-1}), and pCO_2 (µatm) in each season

	Winter	Spring	Summer	Autumn
pH_{NBS}	7.9±0.1	8.1±0.2	8.1±0.1	8.0±0.1
A_T (µmol kg^{-1})	3,256±513	3,114±658	3,185±590	3,280±572
DIC (µmol kg^{-1})	3,291±520	3,095±661	3,120±561	3,290±584
pCO_2 (µatm)	2,063±862	1,489±651	1,216±387	1,924±780

Fig. 7 pCO_2 (µatm) values in relation to apparent oxygen utilization (AOU) in the Guadalquivir estuary

respectively (Table 2). Accordingly, the IE behaved as a strong CO_2 source to the atmosphere, whereas the LE captured CO_2 during certain periods, particularly during the spring and summer months (Fig. 6). Overall, higher fluxes coincided with water discharges from the dam and increased in rainfall (Fig. 4a), although noticeable exchange variability was invariably found in the ME (Fig. 6b). Nevertheless, CO_2 seasonal and annual fluxes were in the same order of magnitude than those measured in other estuarine areas and fell within the range compiled by Chen et al. (2013). In the Guadalquivir estuary in particular, the annual CO_2 flux from 2000 to 2003 calculated by using summer measurements along different sites of the estuary included now in the LE and ME of our division was 37.9 mol C m^{-2} year^{-1} (de la Paz et al., 2007). This value matches quite well that of 36.4± 11.7 mol C m^{-2} year^{-1} obtained in our study for the whole system (Table 3). However, these authors also reported higher instant fluxes (around 114.3–128 mmol C m^{-2} day^{-1}) even though lower pCO_{2water} levels than those found here (Table 1) were present. This discrepancy may be mainly attributed to the average wind speeds, which were manifestly higher in the prior study (7.35 m s^{-1}) as compared to those measured during our sampling period (1.96 m s^{-1}), with less significance on the different k_{600} parameterizations used in both studies. Recently, Morris et al. (2013) provided FCO_2 at the adjacent Doñana wetlands fed by the Guadalquivir River that ranged from 4.1 to 5.5 mmol C m^{-2} day^{-1} and with a mean U_{10} value of

2.5 m s^{-1}, which are in the same order of magnitude than those computed at the LE adjacent to the park (Fig. 6c and Table 3).

The pattern of both pCO_2 and air–water CO_2 exchange suggests that heterotrophy controls the metabolic status of the estuarine waters. Thus, the strong correlation found between pCO_2 and the apparent oxygen utilization (AOU) ($R^2=0.800$, p value<0.001, Fig. 7) indicates that pCO_2 levels were mainly controlled by biological processes, especially organic matter degradation. In the estuary, the organic carbon component was significant, as indicated by the high DOC concentrations measured, with values varying from 1.5 to 14.5 mg l^{-1} (Fig. 8; Table 1). No seasonality was found in the DOC levels (KWRS $\chi^2=95$, $df=3$, p value<0.05), although their spatial distribution revealed a clear variability (KWRS $\chi^2=31.6$, $df=2$, p value<0.001). This finding reflects the effect of mixing as higher DOC concentrations were present upstream in freshwater (Fig. 8) and a more dispersed pattern, with no statistical differences as in the case of turbidity, in the IE and ME (KWMC $p<0.05$; Table 1). Using the criteria described by Abril et al. (2002), according to the average DOC concentration (5.98±2.24 mg l^{-1}, $n=184$), and the considerable

Table 3 Spatiotemporal FCO_2 average values and standard deviation

Zone	Winter flux (mmol C m^{-2} day^{-1})	Spring flux (mmol C m^{-2} day^{-1})	Summer flux (mmol C m^{-2} day^{-1})	Autumn flux (mmol C m^{-2} day^{-1})	Total (mmol C m^{-2} day^{-1})	Annual flux (mol C m^{-2} year^{-1})
LE	12.6±18.7	−0.7±6.9	0.6±3.0	1.0±3.8	3.4±8.1	1.2±0.6
ME	44.5±25.7	28.1±23.8	15.0±10.6	30.2±21.2	29.4±20.3	10.7±1.1
IE	83.9±31.0	60.2±21.0	43.4±10.5	80.2±12.0	66.9±18.6	24.4±1.7
Total	47.0±35.7	29.2±30.5	19.7±21.7	37.1±40.0	99.7±31.9	36.4±11.7
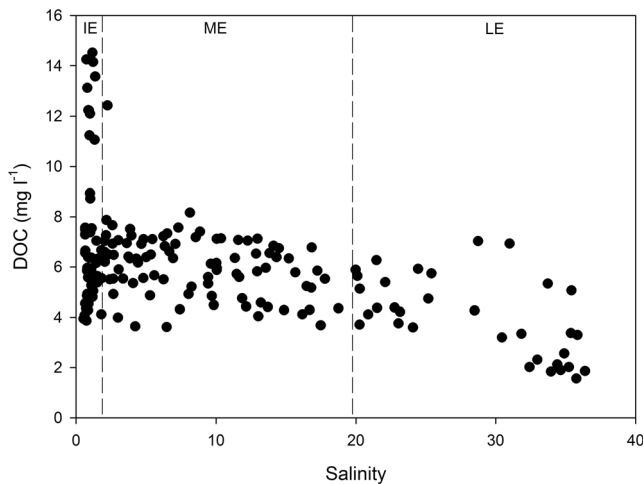
Fig. 8 Dissolved organic carbon (mg l^{-1}) in relation to salinity in the Guadalquivir estuary

anthropogenic pressure over the system (Ruiz et al., 2014), the Guadalquivir estuary can be categorized as heterotrophic and its metabolic status is comparable to that of the Sado and Loire rivers. Another piece of evidence indicative of the heterotrophic status is the inorganic nutrient levels present during the study period (Fig. 9), which were also significantly different for each estuary zone (KWRS $p<0.001$). The highest concentrations of nitrate, nitrite, ammonium, and silicate were found in the IE and ME, with average values around 300, 6, 19, and 100 μM, respectively (Table 1 and Fig. 9a, b, c and e), with a continued decrease towards the river mouth being observed (Fig. 9a, b, c and e). On the other hand, phosphate showed a more homogeneous spatial distribution (Fig. 9d), and average concentrations did not exceed 3 μM (Table 1). Seasonally, only nitrite and phosphate did not present significant variations (KWRS $p>0.05$). Mendiguchía et al. (2007) reported lower nutrient content in the system, particularly for NO_3^-, although sampling was performed twice a year and with river discharges from the dam substantially lower than those observed during our study period.

The stoichiometric ratio N/P evidenced an excess of nitrogen in the system, as values were comprised within the range of 173–1,000, which is, on average, 12 times higher than the optimum Redfield ratio for phytoplankton growth (Redfield 1934). The N/P ratios found here are of the same order of magnitude than those observed in the Pearl River estuary and, in general, characteristic of systems that receive inputs from inland waters enriched in nitrogen relative to phosphorus (Harrison et al. 2009).
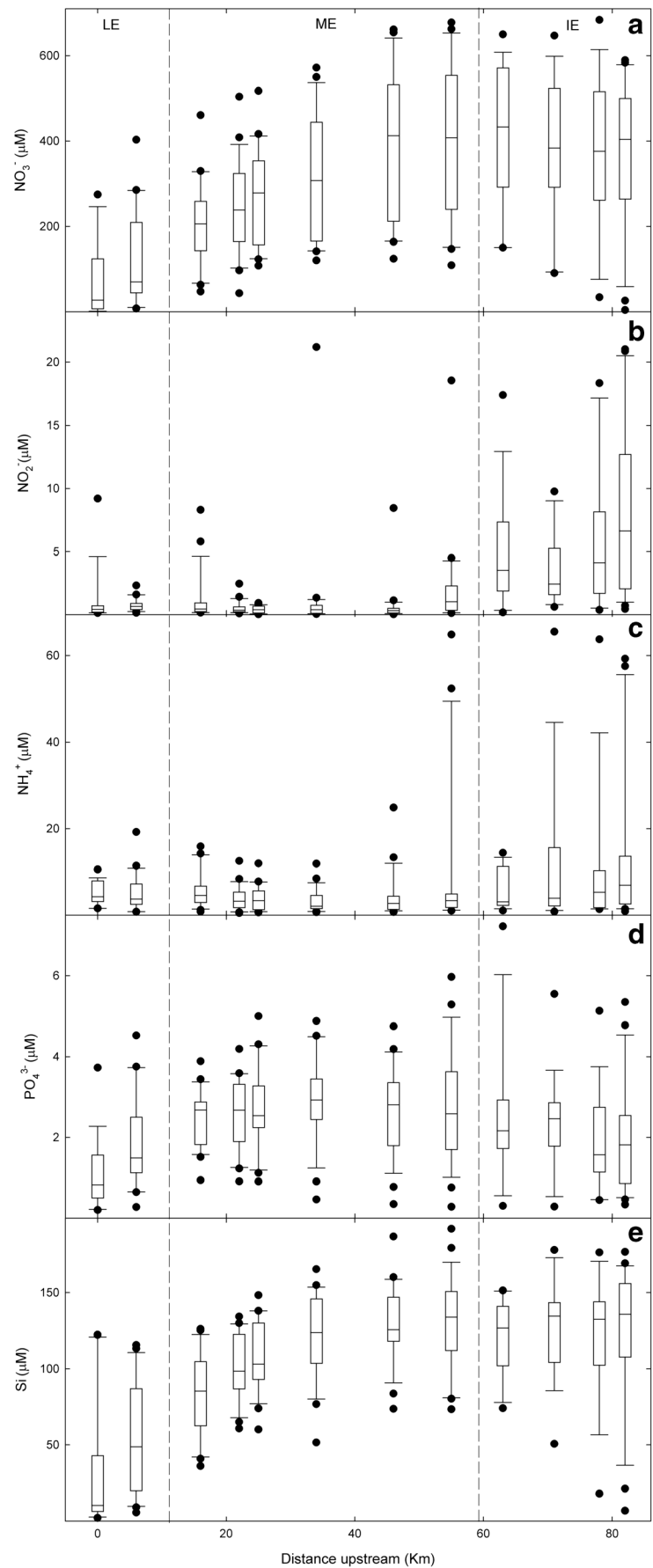
In addition, other processes such as denitrification could partially contribute to the nutrient content in the estuary, particularly because denitrification is favored in heavy turbid

and nitrogen-enriched waters, even under oxic conditions (Liu et al., 2013). From ammonia and nitrate reduction, the nitrification–denitrification process results in increased concentrations of the intermediate NO_2^- component under oxic and anoxic conditions, respectively. Consequently, a rise in N_2O emissions to the atmosphere is commonly observed. In the Guadalquivir estuary, concentrations of NO_3^-, NO_2^-, and NH_4^+ in the ME (MTZ) and the IE (OMZ) were significantly different from those in the LE (KWMC $p<0.05$) and substantially higher (Table 1 and Fig. 9a, b and c), which may be indeed indicative of an enhanced denitrifying microbe activity. In addition, pH_{NBS} values in the IE (7.80± 0.17, Table 1) would favor denitrification (Soetaert et al., 2007), and the elevated A_T measured in this zone (Table 1) would also be indicative of the presence of denitrification, as seen in other anoxic estuaries (Abril and Frankignoulle, 2001). Considering that Ferrón et al. (2010) defined the coastal fringe connected to the Guadalquivir River mouth as a N_2O source to the atmosphere and the highest nitrous oxide saturation concentrations were found at the lowest salinity zone, denitrification may be well claimed as a relevant mechanism participating in the nitrogen balance of the estuary. Nevertheless, further denitrification measurements are required to support this conclusion.

Summary

Our work shows that the high turbid Guadalquivir estuary behaved as a net CO_2 source to the atmosphere during a nearly 2-year period (2007–2009), and a low net gas absorption was only detected in the more saline river mouth during short time intervals. Seasonal variations in the air–water CO_2 fluxes were generally well correlated with an increase in the discharge/rainfall regime in the area, although the permanent heterotrophy in the estuary was the main factor controlling the CO_2 levels in its waters. The very high CO_2 concentrations found in the system and comparable to other high heterotrophic and turbid estuaries were mainly due to the high organic matter and nutrient content (particularly nitrate), which favors respiratory decomposition and denitrification. This status was reflected in a pronounced hypoxia during certain periods and particularly in the inner zone of the estuary, which was also exacerbated by limitation in light penetration, hampering phytoplankton growth and the concomitant water oxygenation. Our data and comparisons with previous records reported in the area confirmed that the Guadalquivir estuary acts as a permanent potent CO_2 emitter to the atmosphere.

Fig. 9 Average concentrations (μM) of inorganic nutrients, **a** nitrate (NO_3^-), **b** nitrite (NO_2^-), **c** ammonium (NH_4^+), **d** phosphate (PO_4^{3-}), **e** and silicate (Si), from the river mouth to 80 upstream during the period of study. The *tops* and *bottoms* of each "box" are the 25th and 75th percentiles of the samples, respectively. The distances between the *tops* and *bottoms* are the interquartile ranges. The *line in the middle of each box* represents the sample median. Observations beyond the whisker length are marked as outliers displayed with a *black dot*

References

Abril, G., and M. Frankignoulle. 2001. Nitrogen–alkalinity interactions in the highly polluted Scheldt basin (Belgium). *Water Research* 35: 844–850.

Abril, G., H. Etcheber, P. Le Hir, P. Bassoullet, B. Boutier, and M. Franki-Gnoulle. 1999. Oxic/anoxic oscillations and organic carbon mineralization in an estuarine maximum turbidity zone (The Gironde, France). *Limnology and Oceanography* 44: 1304–1315.

Abril, G., M. Nogueira, H. Etcheber, G. Cabeçadas, E. Lemaire, and M. Brogueira. 2002. Behaviour of organic carbon in nine contrasting European estuaries. *Estuarine, Coastal and Shelf Science* 54: 241–262.

Ait-Ameur, N., and C. Goyet. 2006. Distribution and transport of natural and anthropogenic CO_2 in the Gulf of Cadiz. *Deep-Sea Research Part Ii-Topical Studies in Oceanography* 53: 1329–1343.

Álvarez-Salgado, X.A., and A.E. Miller. 1998. Simultaneous determination of dissolved organic carbon and total dissolved nitrogen in seawater by high temperature catalytic oxidation: conditions for precise shipboard measurements. *Marine Chemistry* 62: 325–333.

Amann, T., A. Weiss, and J. Hartmann. 2012. Carbon dynamics in the freshwater part of the Elbe estuary, Germany: implications of improving water quality. *Estuarine, Coastal and Shelf Science* 107: 112–121.

Borges, A., and G. Abril. 2011. 5.04-Carbon dioxide and methane dynamics in estuaries. Treatise on estuarine and coastal science, volume 5: biogeochemistry.

Caballero, I., E.P. Morris, J. Ruiz, and G. Navarro. 2013. Assessment of suspended solids in the Guadalquivir estuary using new DEIMOS-1 medium spatial resolution imagery. *Remote Sensing of Environment*.

Cai, W.-J., and Y. Wang. 1998. The chemistry, fluxes, and sources of carbon dioxide in the estuarine waters of the Satilla and Altamaha Rivers, Georgia. *Limnology and Oceanography* 43: 657–668.

Chen, C.-T.A., and A.V. Borges. 2009. Reconciling opposing views on carbon cycling in the coastal ocean: continental shelves as sinks and near-shore ecosystems as sources of atmospheric CO_2. *Deep Sea Research Part II: Topical Studies in Oceanography* 56: 578–590.

Chen, M., S. Wartel, B. Eck, and D. Maldegem. 2005. Suspended matter in the Scheldt estuary. *Hydrobiologia* 540: 79–104.

Chen, C.-T.A., T.-H. Huang, Y.-H. Fu, Y. Bai, and X. He. 2012. Strong sources of CO_2 in upper estuaries become sinks of CO_2 in large river plumes. *Current Opinion in Environmental Sustainability* 4: 179–185.

Chen, C.-T., T.-H. Huang, Y.-C. Chen, Y. Bai, X. He, and Y. Kang. 2013. Air–sea exchanges of CO2 in the world's coastal seas. *Biogeosciences* 10: 6509–6544.

Clark, J.F., P. Schlosser, R. Wanninkhof, H.J. Simpson, W.S.F. Schuster, and D.T. Ho. 1995. Gas transfer velocities for SF_6 and ^{3}He in a small pond at low wind speeds. *Geophysical Research Letters* 22: 93–96.

Conley, D.J., J. Carstensen, R. Vaquer-Sunyer, and C.M. Duarte. 2009. Ecosystem thresholds with hypoxia. In *Eutrophication in Coastal Ecosystems*, 21–29: Springer.

Cox, T., T. Maris, K. Soetaert, D. Conley, S.V. Damme, P. Meire, J.J. Middelburg, M. Vos, and E. Struyf. 2009. A macro-tidal freshwater ecosystem recovering from hypereutrophication: the Schelde case study. *Biogeosciences* 6.

de la Paz, M., A. Gómez-Parra, and J.M. Forja. 2007. Inorganic carbon dynamic and air–water CO_2 exchange in the Guadalquivir Estuary (SW Iberian Peninsula). *Journal of Marine Systems* 68: 265–277.

Dickson, A.G. 1990a. Standard potential of the reaction: AgCl(s) + $12H_2$(g) = Ag(s) + HCl(aq), and the standard acidity constant of the ion HSO$_4$− in synthetic sea water from 273.15 to 318.15 K. *The Journal of Chemical Thermodynamics* 22: 113–127.

Dickson, A.G. 1990b. Thermodynamics of the dissociation of boric acid in synthetic seawater from 273.15 to 318.15 K. *Deep Sea Research Part A. Oceanographic Research Papers* 37: 755–766.

Dickson, A.G., and C. Goyet. 1994. Handbook of methods for the analysis of the various parameters of the carbon dioxide system in sea water. Version 2: Oak Ridge National Lab., TN (United States).

Díez-Minguito, M., A. Baquerizo, M. Ortega-Sánchez, G. Navarro, and M.A. Losada. 2012. Tide transformation in the Guadalquivir estuary (SW Spain) and process-based zonation. *Journal of Geophysical Research, Oceans* 117, C03019.

Díez-Minguito, M., E. Contreras, M.J. Polo, and M.A. Losada. 2013. Spatio-temporal distribution, along-channel transport, and post-riverflood recovery of salinity in the Guadalquivir estuary (SW Spain). *Journal of Geophysical Research, Oceans* 118: 2267–2278.

Etcheber, H., A. Taillez, G. Abril, J. Garnier, P. Servais, F. Moatar, and M.-V. Commarieu. 2007. Particulate organic carbon in the estuarine turbidity maxima of the Gironde, Loire and Seine estuaries: origin and lability. *Hydrobiologia* 588: 245–259.

Ferrón, S., T. Ortega, and J.M. Forja. 2010. Nitrous oxide distribution in the north-eastern shelf of the Gulf of Cádiz (SW Iberian Peninsula). *Marine Chemistry* 119: 22–32.

Flecha, S., F.F. Pérez, G. Navarro, J. Ruiz, I. Olivé, S. Rodríguez-Gálvez, E. Costas, and I.E. Huertas. 2012. Anthropogenic carbon inventory in the Gulf of Cádiz. *Journal of Marine Systems* 92: 67–75.

Frankignoulle, M., G. Abril, A. Borges, I. Bourge, C. Canon, B. Delille, E. Libert, and J.-M. Théate. 1998. Carbon dioxide emission from European estuaries. *Science* 282: 434–436.

Gaillardet, J., B. Dupré, and C.J. Allègre. 1999. Geochemistry of large river suspended sediments: silicate weathering or recycling tracer? *Geochimica et Cosmochimica Acta* 63: 4037–4051.

Gallegos, C.L. 2001. Calculating optical water quality targets to restore and protect submersed aquatic vegetation: overcoming problems in partitioning the diffuse attenuation coefficient for photosynthetically active radiation. *Estuaries* 24: 381–397.

Garnier, J., G. Billen, J. Némery, and M. Sebilo. 2010. Transformations of nutrients (N, P, Si) in the turbidity maximum zone of the Seine estuary and export to the sea. *Estuarine, Coastal and Shelf Science* 90: 129–141.

Gattuso, J.P., M. Frankignoulle, and R. Wollast. 1998. Carbon and carbonate metabolism in coastal aquatic ecosystems. *Annual Review of Ecology and Systematics* 29: 405–434.

Giradoux, P. 2012. pgirmess: data analysis in ecology. R package version 1.5.4. http://CRAN.R-project.org/package=pgirmess.

Grasshoff, K., M. Erhardt, and K. Kremling. 1983. Methods of seawater analysis. 2. *Acta Hydrochimica et Hydrobiologica* 14: 79–80.

Harrison, J.A., R.J. Maranger, R.B. Alexander, A.E. Giblin, P.A. Jacinthe, E. Mayorga, S.P. Seitzinger, D.J. Sobota, and W.M. Wollheim.

2009. The regional and global significance of nitrogen removal in lakes and reservoirs. *Biogeochemistry* 93: 143–157.

Herman, P.M., and C.H. Heip. 1999. Biogeochemistry of the MAximum TURbidity Zone of Estuaries (MATURE): some conclusions. *Journal of Marine Systems* 22: 89–104.

Huertas, I.E., G. Navarro, S. Rodríguez-Gálvez, and L.M. Lubián. 2006. Temporal patterns of carbon dioxide in relation to hydrological conditions and primary production in the northeastern shelf of the Gulf of Cadiz (SW Spain). *Deep Sea Research Part II: Topical Studies in Oceanography* 53: 1344–1362.

Husson, F., J. Josse, S. Le, and J. Mazet. 2012. FactoMineR: multivariate exploratory data analysis and data mining with R. In package = FactoMineR.R package version 1.19. http://CRAN.R-project.org/

Jiang, L.-Q., W.-J. Cai, and Y. Wang. 2008. A comparative study of carbon dioxide degassing in river- and marine-dominated estuaries. *Limnology and Oceanography* 53: 2603–2615.

Kim, T.W., K. Lee, R.A. Feely, C.L. Sabine, C.T.A. Chen, H.J. Jeong, and K.Y. Kim. 2010. Prediction of Sea of Japan (East Sea) acidification over the past 40 years using a multiparameter regression model. *Global Biogeochemical Cycles* 24.

Kirk, J.T.O. 1994. *Light and photosynthesis in aquatic ecosystems*: Cambridge University Press.

Knap, A., A. Michaels, A. Close, H. Ducklow, and A. Dickson. 1996a. Protocols for the Joint Global Ocean Flux Study (JGOFS) core measurements. *JGOFS, Reprint of the IOC Manuals and Guides No. 29, UNESCO 1994* 19.

Knap, A.H., A. Michaels, A.R. Close, H. Ducklow, and A.G. Dickson. 1996b. *Protocols for the Joint Global Ocean Flux Study (JGOFS) core measurements*.

Laruelle, G.G., H.H. Dürr, C.P. Slomp, and A.V. Borges. 2010. Evaluation of sinks and sources of CO2 in the global coastal ocean using a spatially-explicit typology of estuaries and continental shelves. *Geophysical Research Letters* 37.

Lee, K., T.-W. Kim, R.H. Byrne, F.J. Millero, R.A. Feely, and Y.-M. Liu. 2010. The universal ratio of boron to chlorinity for the North Pacific and North Atlantic oceans. *Geochimica et Cosmochimica Acta* 74: 1801–1811.

Lewis, E., D. Wallace, and L.J. Allison. 1998. *Program developed for CO2 system calculations*: Carbon Dioxide Information Analysis Center, managed by Lockheed Martin Energy Research Corporation for the US Department of Energy.

Liu, T., X. Xia, S. Liu, X. Mou, and Y. Qiu. 2013. Acceleration of denitrification in turbid rivers due to denitrification occurring on suspended sediment in oxic waters. *Environmental Science & Technology* 47: 4053–4061.

Mann, K.H. 1982. *Ecology of coastal waters: a systems approach*. University of California Press.

Memoria 2009/2011, ed. C.H.d. Guadalquivir: Ministerio de Agricultura, Alimentación y Medio Ambiente, Gobierno de España.

Mendiguchía, C., C. Moreno, and M. García-Vargas. 2007. Evaluation of natural and anthropogenic influences on the Guadalquivir River (Spain) by dissolved heavy metals and nutrients. *Chemosphere* 69: 1509–1517.

Mintrop, L., A. Kortzinger, and J.C. Duinker. 1999. The carbon dioxide system in the northwestern Indian Ocean during south-west monsoon. *Marine Chemistry* 64: 315–336.

Morris, E.P., S. Flecha, J. Figuerola, E. Costas, G. Navarro, J. Ruiz, P. Rodriguez, and E. Huertas. 2013. Contribution of Doñana wetlands to carbon sequestration. *PLoS One* 8: e71456.

Navarro, G., F. Gutiérrez, M. Díez-Minguito, M. Losada, and J. Ruiz. 2011. Temporal and spatial variability in the Guadalquivir estuary: a challenge for real-time telemetry. *Ocean Dynamics* 61: 753–765.

Navarro, G., I.E. Huertas, E. Costas, S. Flecha, M. Díez-Minguito, I. Caballero, V. López-Rodas, L. Prieto, and J. Ruiz. 2012. Use of a real-time remote monitoring network (RTRM) to characterize the Guadalquivir estuary (Spain). *Sensors* 12: 1398–1421.

Pérez-Hidalgo, T., and J. Trinidad. 2004. Cuencas cenozoicas. In *Geología de España*, ed. I.G.y.M.d. España

R Development Core Team. 2013. *R: a language and environment for statistical computing*. Vienna, Austria: R Foundation for Statistical Computing.

Raymond, P., and J. Cole. 2001. Gas exchange in rivers and estuaries: choosing a gas transfer velocity. *Estuaries and Coasts* 24: 312–317.

Redfield, A.C. 1934. *On the proportions of organic derivatives in sea water and their relation to the composition of plankton*: University Press of Liverpool.

Ribas-Ribas, M., A. Gómez-Parra, and J.M. Forja. 2011. Air–sea CO_2 subfluxes in the north-eastern shelf of the Gulf of Cádiz (southwest Iberian Peninsula). *Marine Chemistry* 123: 56–66.

Ribas-Ribas, M., E. Anfuso, A. Gómez-Parra, and J.M. Forja. 2013. Tidal and seasonal carbon and nutrient dynamics of the Guadalquivir estuary and the Bay of Cádiz (SW Iberian Peninsula). *Biogeosciences* 10: 4481–4491.

Richey, J.E., A.H. Devol, S.C. Wofsy, R. Victoria, and M.N. Riberio. 1988. Biogenic gases and the oxidation and reduction of carbon in Amazon River and floodplain waters. *Limnology and Oceanography* 33: 551–561.

Ruiz, J. 2010. Capítulo 7: Ciclos biogeoquímicos del estuario: Impacto sobre la Biota, la Biodiversidad y la Toxicidad. In Propuesta metodológica para diagnosticar y ponosticar las consecuencias de las actuaciones humanas en el estuario del Guadalquivir., ed. A.P.d. Sevilla: Instituto de Ciencias Marinas de Andalucia (ICMAN-CSIC).

Ruiz, J., R. González-Quirós, L. Prieto, and G. Navarro. 2009. A Bayesian model for anchovy (Engraulis encrasicolus): the combined forcing of man and environment. *Fisheries Oceanography* 18: 62–76.

Ruiz, J., M.J. Polo, M. Díez-Minguito, G. Navarro, E.P. Morris, E. Huertas, I. Caballero, E. Contreras, and M.A. Losada. 2014. The Guadalquivir estuary: a hot spot for environmental and human conflicts. In *Advances in coastal and marine resources: remote sensing and modeling*, ed. C.W. Finkl: Submitted

Sharp, J.H. 2010. Estuarine oxygen dynamics: what can we learn about hypoxia from long-time records in the Delaware Estuary? *Limnology and Oceanography* 55: 535.

Smith, S.D. 1988. Coefficients for sea surface wind stress, heat flux, and wind profiles as a function of wind speed and temperature. *Journal of Geophysical Research, Oceans* 93: 15467–15472.

Soetaert, K., J.J. Middelburg, C. Heip, P. Meire, S. Van Damme, and T. Maris. 2006. Long-term change in dissolved inorganic nutrients in the heterotrophic Scheldt estuary (Belgium, The Netherlands). *Limnology and Oceanography* 51: 409–423.

Soetaert, K., A.F. Hofmann, J.J. Middelburg, F.J.R. Meysman, and J. Greenwood. 2007. The effect of biogeochemical processes on pH. *Marine Chemistry* 105: 30–51.

Taglialatela, S., L. Prieto, G. Navarro, and J. Ruiz Segura. 2012. Annual patterns in mesozooplankton distribution along the salinity gradient in the Guadalquivir Estuary. *Estuarine, Coastal and Shelf Science* 149: 244–254.

Testa, J.M., W.M. Kemp, C.S. Hopkinson, and S.V. Smith. 2013. *Ecosystem metabolism*, 381–416. Second Edition: Estuarine Ecology.

Vaquer-Sunyer, R., and C.M. Duarte. 2008. Thresholds of hypoxia for marine biodiversity. *Proceedings of the National Academy of Sciences* 105: 15452–15457.

Wanninkhof, R. 1992. Relationship between wind speed and gas exchange. *Journal of Geophysical Research* 97: 7373–7382.

Wanninkhof, R., W.E. Asher, D.T. Ho, C. Sweeney, and W.R. McGillis. 2009. Advances in quantifying air-sea gas exchange and environmental forcing. *Annual Review of Marine Science* 1: 213–244.

Weiss, R.F. 1974. Carbon dioxide in water and seawater: the solubility of a non-ideal gas. *Marine Chemistry* 2: 203–215.

Weiss, R., and B. Price. 1980. Nitrous oxide solubility in water and seawater. *Marine Chemistry* 8: 347–359.